ACS OMEGA

http://pubs.acs.org/journal/acsodf

Article

Enhanced Adsorption of Rhodamine B on Modified Oil-Based Drill Cutting Ash: Characterization, Adsorption Kinetics, and Adsorption Isotherm

Yuqing Zhao, Hang Yang, Jianfa Sun, Yi Zhang,* and Shibin Xia*

Cite This: *ACS Omega* 2021, 6, 17086−17094

Read Online

ACCESS | Metrics & More | Article Recommendations

ABSTRACT: In this paper, phosphoric acid (H_3PO_4), hydrochloric acid (HCl), and hydrogen peroxide (H_2O_2) were employed for the modification of oil-based drill cutting ash (OBDCA) for the first time. The adsorption of rhodamine B (RhB) on modified oil-based drill cutting ash (MOBDCA) in an aqueous medium was investigated. H_2O_2-modified OBDCA had the optimal adsorption efficiency for RhB. The physical and chemical properties of MOBDCA were analyzed using X-ray diffraction (XRD), scanning electron microscopy (SEM), Fourier transform infrared spectroscopy (FTIR), ζ-potential, N_2 adsorption−desorption isotherm, and pore size distribution. The effect of the pH value (3−11), reaction time (10−720 min), and initial RhB concentration (10−200 mg/L) on RhB adsorption was discussed. The adsorption kinetics highly fitted with the pseudo-second-order model ($R^2 > 0.99$), which indicated that the adsorption process was dominated by chemisorption. The adsorption isotherm fitted well with the Langmuir and Freundlich models ($R^2 > 0.97$), which indicated the monolayer adsorption process and the heterogeneous adsorption process, respectively. The theoretic adsorption capacity (50 mg/g) for RhB was achieved by H_2O_2-modified OBDCA. This paper provides a promising method of resource utilization of OBDCA to treat organic pollutants.

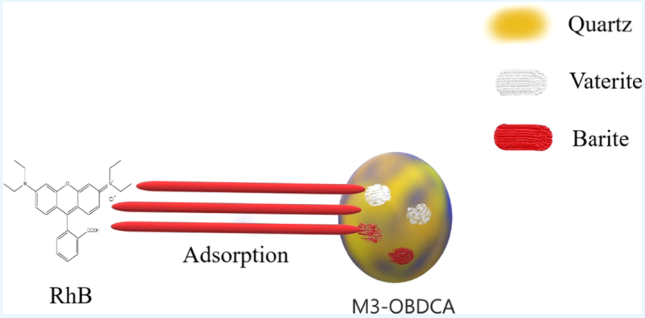

INTRODUCTION

With the rapid development of industry, more and more industrial wastewater is discharged into the environment without sufficient treatment, resulting in increasingly serious pollution of water resources.[1,2] Common pollutants in the water environment include organic dyes, heavy metals, pesticides, antibiotics, and hormone drugs.[3−5] Among them, dyes are the main source of water pollution, which are widely used in papermaking, textile, leather, printing, and dyeing industries.[6−10] Rhodamine B (RhB), a xanthene-type cationic dye, is commonly used in rubber, paper, and plastic manufacturing industries.[11−13] Insufficient treatment for RhB in water bodies could result in environmental pollution and cause harm to human health.[14] Therefore, the removal of RhB is of great significance.

The main methods for treating dyes in wastewater include adsorption, flocculation, chemical oxidation, reverse osmosis, photocatalytic degradation, and so on.[15−19] Among them, adsorption technology has attracted much attention due to its advantages such as simplicity, eco-friendliness, and recyclability of adsorbents.[20,21] Traditional materials used to adsorb dyes usually include zeolite, biological materials, nanomaterials, carbonaceous materials, ion exchange resins, and so on.[22−24]

Oil-based drill cutting ash (OBDCA) is a solid waste that is produced from the pyrolysis product of oil-based drill cuttings (OBDC). In China, the yield of OBDCA is up to 200 thousand tons, which cannot be fully utilized due to the huge quantity. The main utilization method of OBDCA is as a raw material for brick and cement.[25−27] In our previous study, OBDCA was developed as a novel material of environmental remediation for metal polluted soil and water.[28,29] However, OBDCA is currently not used in the removal of organic matter due to the poor adsorption efficiency for organic matter. To enhance adsorption for organic matter, appropriate modification of OBDCA should be studied. Acid modifications have been widely used to improve the adsorption capacity of the material for pollutants. The possible reasons are that acid modification could remove soluble salts, introduce new functional groups, increase the pore volume, and enhance the specific surface area for the material.[30−32] In this study,

Received: April 27, 2021
Accepted: June 17, 2021
Published: June 25, 2021

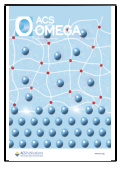

https://doi.org/10.1021/acsomega.1c02214
ACS Omega 2021, 6, 17086−17094

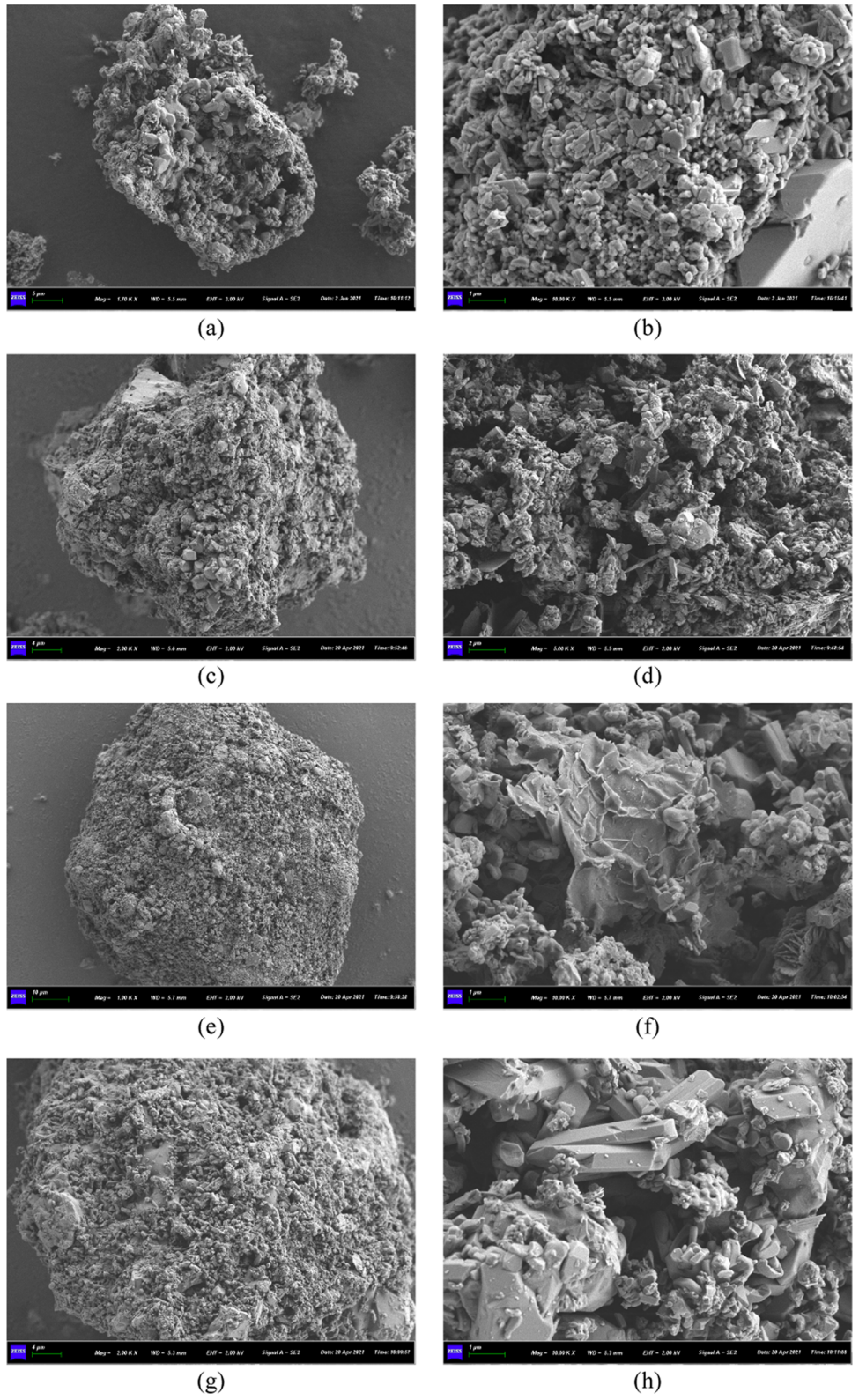

Figure 1. SEM photographs of the samples: (a, b) OBDCA, (c, d) M1-OBDCA, (e, f) M1-OBDCA, and (g, h) M1-OBDCA.

three common acids, H_3PO_4, HCl, and H_2O_2 were selected to modify OBDCA for improving the adsorption capacity for organic pollutants.

The main aims of this study were (1) to modify OBDCA using three acids; (2) to compare the characterization of modified OBDCA (MOBDCA) and OBDCA; (3) to investigate the effect of the modification method and pH value on RhB removal; and (4) to study the adsorption kinetics and adsorption isotherm of RhB on MOBDCA and OBDCA.

Characterization of OBDCA and MOBDCA. The morphology characterization of OBDCA and MOBDCA was analyzed using a scanning electron microscope (SEM) (Figure

https://doi.org/10.1021/acsomega.1c02214
ACS Omega 2021, 6, 17086−17094

1). OBDCA was an irregular particle with a relatively coarse surface structure, which indicated the presence of impurity on OBDCA. For M1-OBDCA, the morphology of M1-OBDCA had no obvious difference with OBDCA. For M2-OBDCA and M3-OBDCA, the morphology of the two samples was an irregular particle shape with a relatively smooth surface structure, which indicated less impurity on OBDCA. The change of morphology was due to the stronger oxidation and corrosion effect of HCl and H_2O_2 than H_3PO_4 for OBDCA modification.

The surface functional group of OBDCA and MOBDCA was analyzed using Fourier transform infrared spectroscopy (FTIR; Figure 2). For OBDCA, the obvious band appeared at

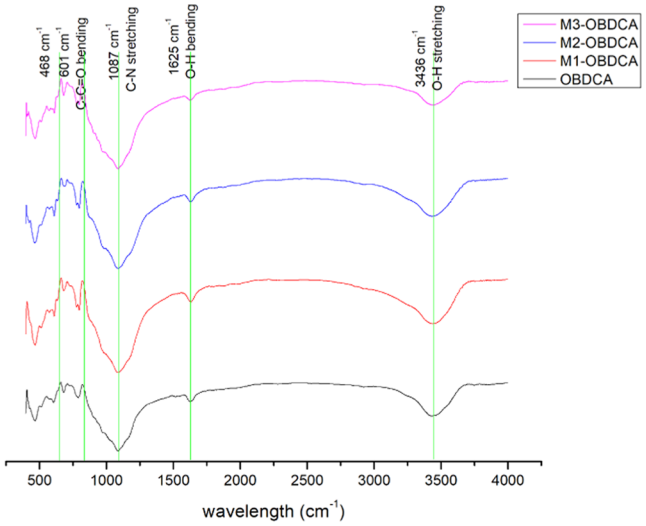

Figure 2. FTIR spectra of MOBDCA and OBDCA.

3436 cm^{-1} was attributed to the O−H stretching vibration peak;[33] the band appeared at 1625 cm^{-1} was attributed to O−H bending vibration peak.[34] The band appeared at 1087 cm^{-1} was attributed to the C−N stretching vibration peak.[35] The bands appeared at 601−468 cm^{-1} were ascribed to C−C═O stretching vibration peaks.[36] The FTIR spectra of the three modified OBDCA samples had no obvious difference compared with those of OBDCA, which indicated that modification had not changed the functional group for OBDCA.

The composition of OBDCA and MOBDCA was analyzed using X-ray diffraction (XRD) (Figure 3). For OBDCA, many mess peaks appeared in the XRD pattern of OBDCA, which indicated the complex composition of OBDCA. According to the index result, the main diffraction planes observed in OBDCA included quartz (SiO_2, PDF 79-1907), barite ($BaSO_4$, PDF 76-0213), and vaterite ($CaCO_3$, PDF 74-1816).[37−39] For M1-OBDCA and M3-OBDCA, the XRD pattern had no obvious difference compared with that of OBDCA. For M2-OBDCA, the diffraction planes corresponding to barite and vaterite disappeared. This was due to the reaction of $CaCO_3$ with HCl to form $CaCl_2$, which resulted in the reduction of vaterite in M2-OBDCA. In addition, although $BaSO_4$ could not react with HCl, the solubility of $BaSO_4$ increased in the presence of HCl, which also resulted in the reduction of barite in M2-OBDCA.

Figure 4 shows the N_2 adsorption/desorption isotherms and pore size distributions of OBDCA and MOBDCA. For

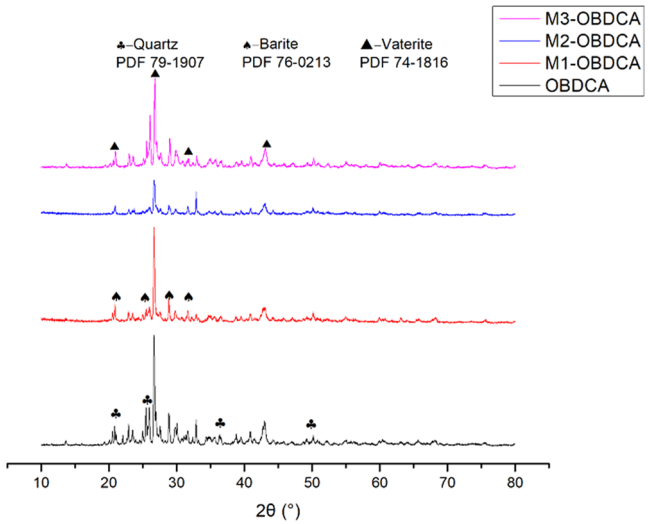

Figure 3. XRD patterns of MOBDCA and OBDCA.

OBDCA, according to the Brunauer−Deming−Deming−Teller (BDDT) classification, the N_2 adsorption/desorption isotherms of OBDCA were irreversible approximate type II with no obvious hysteresis loop; the data of pore size distribution indicated the non-porous structure of OBDCA with a very small pore volume. For M1-OBDCA and M3-OBDCA, N_2 adsorption/desorption isotherms and pore size distributions were similar to those of OBDCA. For M2-OBDCA, the N_2 adsorption/desorption isotherms of OBDCA were irreversible approximate type II with an obvious hysteresis loop; despite the relatively high pore volume, the data of pore size distribution still indicated the non-porous structure of M3-OBDCA due to the small total pore volume. According to the result of the BET parameter (Table 1), the order of the surface area and total pore volume was as follows: OBDCA < M3-OBDCA < M1-OBDCA < M2-OBDCA. The highest surface area was obtained for M2-OBDCA due to the reduction of barite, vaterite, and other impurities after HCl modification.

The colloidal dispersion stability and potential value under different pH values were analyzed using ζ-potential analysis (Figure 5). The obtained pH_{pzc} values for OBDCA and MOBDCA were all less than 3.0, which indicated the negative charge on the surface of OBDCA and MOBDCA when pH > 3.0.

RESULTS AND DISCUSSION

Figure 6a shows the effect of the modification method of OBDCA on RhB adsorption. Three modified OBDCA samples had higher adsorption capacity for RhB than OBDCA. The order of the removal rate for RhB was as follows: OBDCA (60.1%) < M2-OBDCA (75.0%) < M1-OBDCA (76.3%) < M3-OBDCA (81.3%). The conclusion was not consistent with the BET surface area of the adsorbent. Especially, M2-OBDCA with the highest BET surface area had little enhanced adsorption capacity compared with OBDCA. This was possible due to the discussion mentioned in XRD patterns. HCl modification could corrode the surface of OBDCA to generate more adsorption sites for RhB adsorption. However, barite, vaterite, and other impurities in OBDCA, which could also adsorb the dye at a certain degree, were also reduced after HCl modification.[40−42] The H_3PO_4 and H_2O_2 modification could

https://doi.org/10.1021/acsomega.1c02214
ACS Omega 2021, 6, 17086−17094

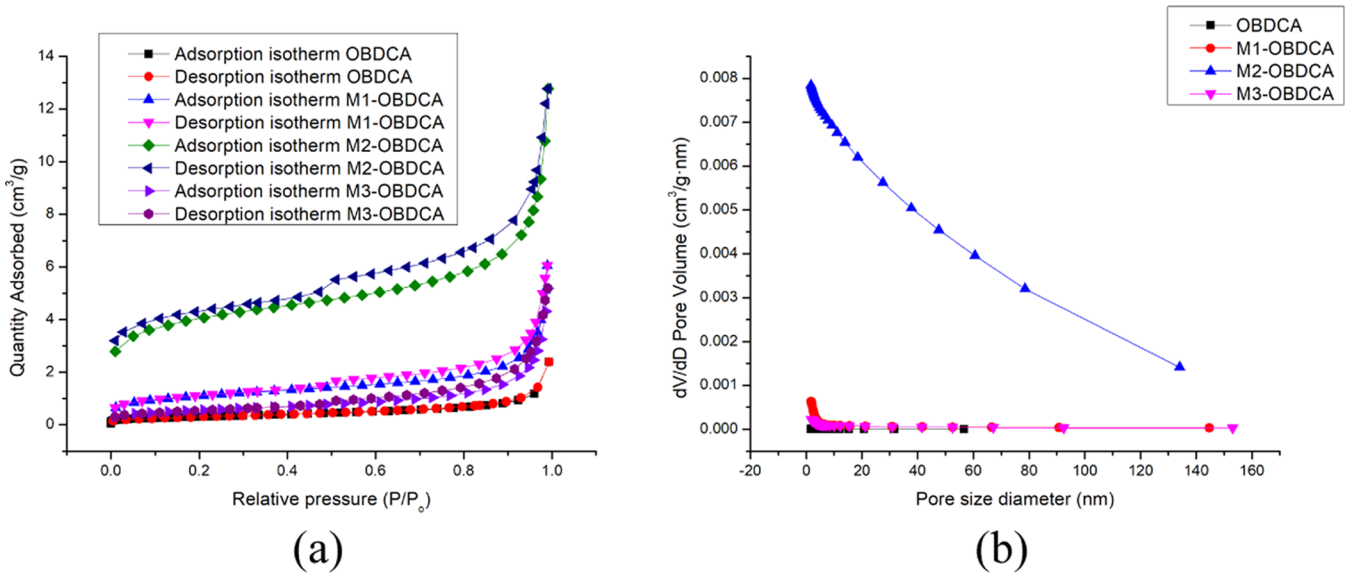

Figure 4. BET analysis of MOBDCA and OBDCA: (a) N_2 isotherm and (b) pore size distribution.

Table 1. Brunauer–Emmett–Teller (BET) Parameters of MOBDCA and OBDCA

	BET surface area (m^2/g)	total volume (cm^3/g)	average pore diameter (nm)
OBDCA	1.0993	0.0037	13.4
M1-OBDCA	3.8590	0.0093	9.7
M2-OBDCA	14.5641	0.0197	5.2.
M3-OBDCA	1.9371	0.0080	12.6

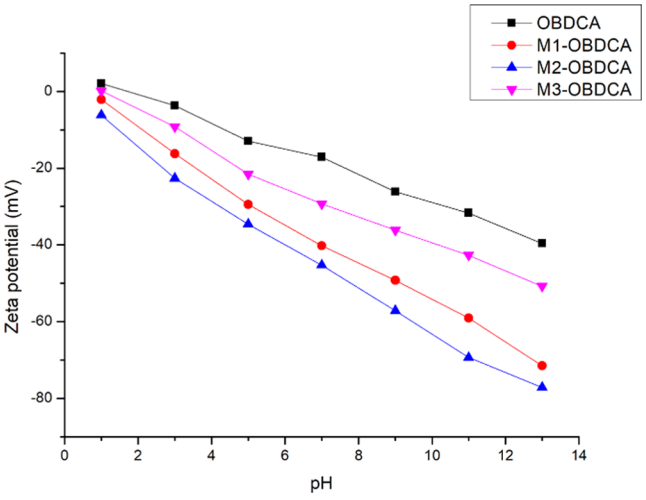

Figure 5. ζ-Potential measurement of OBDCA and MOBDCA under different pH values.

oxidize and corrode the surface of OBDCA with relatively intact retention of barite and vaterite. In addition, among the three MOBDCA, M3-OBDCA had the lowest BET surface area and the optimal adsorption efficiency for RhB, which could indicate that the H_2O_2 modification could enhance the hydrophilicity and affinity of OBDCA for RhB.[43]

Figure 6b shows the effect of pH on RhB adsorption. For the four adsorbents, the pH value had an obvious effect on the removal rate of RhB, and the removal rate increased with increasing pH value. This was because (i) RhB is a weakly basic dye, which has a positive surface charge.[44] (ii) According to the result of the ζ-potential analysis of the adsorbent, the surface charge of the adsorbent was negative when pH > 3, while there was a strong electrostatic attraction between the adsorbent and the RhB solution when pH > 3. Therefore, a higher pH value was conducive for RhB adsorption due to the more obvious electrostatic attraction.

Adsorption Kinetics and Adsorption Isotherm. The pseudo-first-order model, pseudo-second-order model, and intraparticle diffusivity model were employed to determine the kinetic mechanism of the adsorption process.[45,46] The kinetic plots and the corresponding parameters are shown in Figure 7 and Table 2, respectively. According to the calculated coefficients (R^2), the pseudo-second-order kinetic model was more suitable to explain the adsorption process of RhB on the adsorbent, which indicated that the main adsorption process was controlled by chemisorption. The intraparticle diffusivity model was also suitable to fit the adsorption process. As shown in Figure 7c, the intraparticle diffusivity plot was divided into two steps ((I) and (II)). For the first (I) step, the experiment data had a high coefficient and the fitted curve was close to the origin, which indicated that this step was mainly controlled by intraparticle diffusivity.[47] For the second (II) step, the experiment data had a low coefficient and the fitted curve was far from the origin, which indicated that this step was mainly controlled by extraparticle diffusivity.

The Langmuir and Freundlich models were employed to fit the adsorption isotherm of RhB on the adsorbent.[48,49] The isotherm plots and the corresponding parameters are shown in Figure 8 and Table 3, respectively. According to the calculated coefficients (R^2), the Langmuir and Freundlich isotherm models were both suitable to explain the adsorption process of RhB on the adsorbent. The parameters k_l (<1) and n (<1) indicated the homogeneous, monolayer, and favorable adsorption process. The theoretic adsorption capacity, Q_m, was calculated from the Langmuir equation in the following order: OBDCA (18 mg/g) < M2-OBDCA (21 mg/g) < M1-OBDCA (30 mg/g) < M3-OBDCA (50 mg/g).

Comparison with Other Adsorbents for RhB. The adsorption capacity of M3-OBDCA for RhB was compared

https://doi.org/10.1021/acsomega.1c02214
ACS Omega 2021, 6, 17086−17094

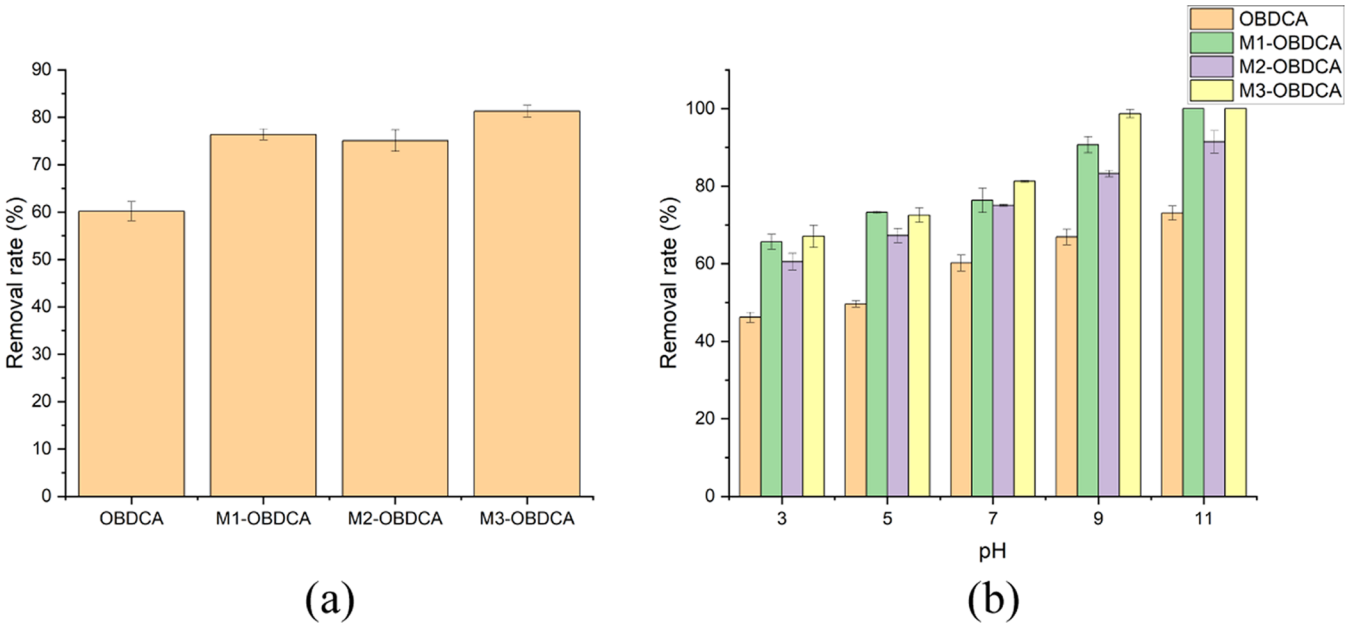

Figure 6. (a) Effect of the modification method of OBDCA on the removal rate of RhB. Experimental conditions: dosage of the adsorbent: 1 g/L, pH: 7, reaction time: 180 min, and initial RhB concentration: 10 mg/L. (b) Effect of the pH value on the removal rate of RhB. Experimental conditions: dosage of the adsorbent: 1 g/L, pH: 3−11, reaction time: 180 min, and initial RhB concentration: 10 mg/L.

with other adsorbents (Table 4). The adsorption capacity of M3-OBDCA was not at a high level compared with some adsorbents. Different from other adsorbents, OBDCA is a solid waste and the modification of OBDCA was very low cost. Meanwhile, the use of M3-OBDCA for RhB adsorption achieved waste utilization, which had a certain environmental significance. However, the regeneration of used M3-OBDCA may result in secondary environmental pollution and disproportionate cost consumption. The used M3-OBDCA was considered to be utilized and developed to prepare other materials, such as bricks, cement-based materials, and proppants.[25,26,50]

EXPERIMENTAL SECTION

Materials and Instruments. Materials: OBDC was provided by Agriculture and Forestry Department of Fuling Shale Gas Company. OBDCA was obtained by pyrolysis of OBDC. The pyrolysis conditions were as follows: pyrolysis temperature was 750 °C, pyrolysis time was 45 min, and heating rate was 6 °C/min. OBDCA was ground and sieved through a 200-mesh screen. Phosphoric acid (H_3PO_4), hydrochloric acid (HCl), rhodamine B (RhB), hydrogen peroxide (H_2O_2), and (NaOH) were bought from Aladdin Company.

Instruments: An automatic surface area and porosity analyzer (ASAP 2020M) was used to analyze the N_2 adsorption isotherms and pore size distribution of the samples. A ζ-potential analyzer (NanoPlus) was used to analyze the ζ-potential of the samples. An X-ray diffractometer (D8 Advance) was used to analyze the X-ray diffraction (XRD) pattern of the samples. A field emission scanning electron microscope (FE-SEM; JSM-IT300) was used to measure the surface morphologies of the samples. A Fourier transform infrared spectrometer (Nexus) was used to analyze the Fourier transform infrared spectroscopy (FTIR) spectrum of the samples.

Modification of OBDCA. H_3PO_4, HCl, and H_2O_2 were used for OBDCA modification. In the modification process, 20 g of OBDCA was added into each 1000 mL conical flask with 800 mL of a H_3PO_4 (30%) solution, 800 mL of a HCl (10%) solution, and 800 mL of a H_2O_2 (30%) solution, separately. Then, the conical flasks were sealed and shaken in a shaker for 24 h at 25 °C. Modified OBDCA was collected and rinsed using ultrapure water until the pH was neutral. The modified OBDCA was dried using a dryer for 24 h at 120 °C. H_3PO_4-, HCl-, and H_2O_2-modified OBDCA were denoted as M1-OBDCA, M2-OBDCA, and M3-OBDCA, respectively.

Adsorption Experiment. Adsorption tests were carried out using batch experiments. OBDCA (0.1 g) was added into 150 mL conical flasks with 100 mL of the RhB solution. H_2SO_4 (0.1 mol/L) and NaOH (0.1 mol/L) were used to adjust the pH value. Then, the conical flasks were sealed and shaken in a shaker for 3 h at 25 °C. After adsorption, the RhB aqueous solution was filtered using a syringe filter to remove the OBDCA residue. The concentration of RhB in the filtrate was measured using an ultraviolet spectrometer at λ_{max} wavelength of HA (wavelength: 554 nm). The removal rate (%) and unit adsorption quantity (mg/g) of RhB were calculated according to eqs 1 and 2, respectively. All experiments were carried out three times at least.

$$\text{removal rate} = \frac{C_0 - C_t}{C_0} \times 100\% \quad (1)$$

$$\text{unit adsorption quantity} = \frac{(C_0 - C_t)V}{W} \quad (2)$$

where C_0 and C_t are the initial concentration (mg/L) and residue concentration (mg/L) after the adsorption of RhB, respectively; V is the volume of the solution (L); and W is the weight of the dosage of the adsorbent (g).

The adsorption kinetics of RhB on OBDCA was fitted with the pseudo-first-order, pseudo-second-order, and intraparticle diffusivity models (eqs 3−5, respectively).

https://doi.org/10.1021/acsomega.1c02214
ACS Omega 2021, 6, 17086−17094

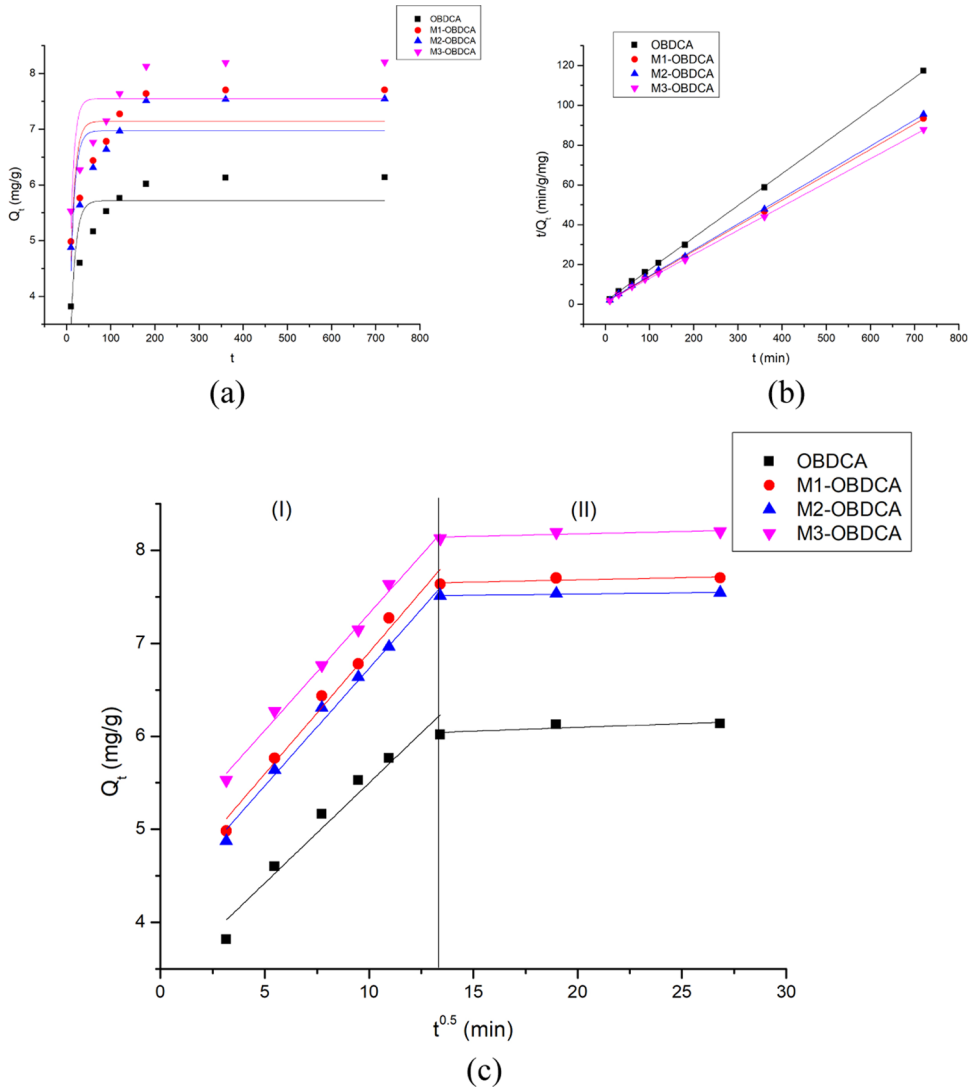

Figure 7. (a) Pseudo-first-order, (b) pseudo-second-order, and (c) intraparticle diffusivity model plots. Experimental conditions: dosage of the adsorbent: 1 g/L, pH: 7, reaction time: 10−720 min, and initial RhB concentration: 10 mg/L.

Table 2. Adsorption Kinetic Model Parameters

	pseudo-first-order		
	k_1 (min^{-1})	q_m (mg/g)	R^2
OBDCA	0.09 ± 0.01	5.7 ± 0.1	0.6434
M1-OBDCA	0.10 ± 0.01	7.1 ± 0.3	0.5446
M2-OBDCA	0.10 ± 0.01	6.9 ± 0.4	0.5391
M3-OBDCA	0.11 ± 0.01	7.5 ± 0.6	0.4644
	pseudo-second-order		
	q_e (mg/g)	k_2 (g/mg/min)	R^2
OBDCA	6.0 ± 0.2	0.017 ± 0.001	0.9998
M1-OBDCA	7.8 ± 0.3	0.013 ± 0.001	0.9997
M2-OBDCA	7.6 ± 0.2	0.013 ± 0.001	0.9970
M3-OBDCA	8.3 ± 0.2	0.012 ± 0.001	0.9967
	intraparticle diffusivity		
	k_w (min^{-1})	b	R^2
OBDCA	0.21 ± 0.01 (I)/0.0082 ± 0.0004(II)	3.3 ± 0.3 (I)/5.9 ± 0.3 (II)	0.9473 (I)/0.4541 (II)
M1-OBDCA	0.26 ± 0.03(I)/0.0043 ± 0.0006(II)	4.3 ± 0.2 (I)/7.6 + 0.5 (II)	0.9805 (I)/0.3683 (II)
M2-OBDCA	0.23 ± 0.03 (I)/0.0027 ± 0.0003(II)	4.2 + 0.3 (I)/7.4 + 0.6 (II)	0.9861 (I)/0.8207 (II)
M3-OBDCA	0.25 ± 0.02(I)/0.0052 ± 0.0004(II)	4.8 + 0.3 (I)/8.1 + 0.7(II)	0.9931 (I)/0.4531 (II)

https://doi.org/10.1021/acsomega.1c02214
ACS Omega 2021, 6, 17086−17094

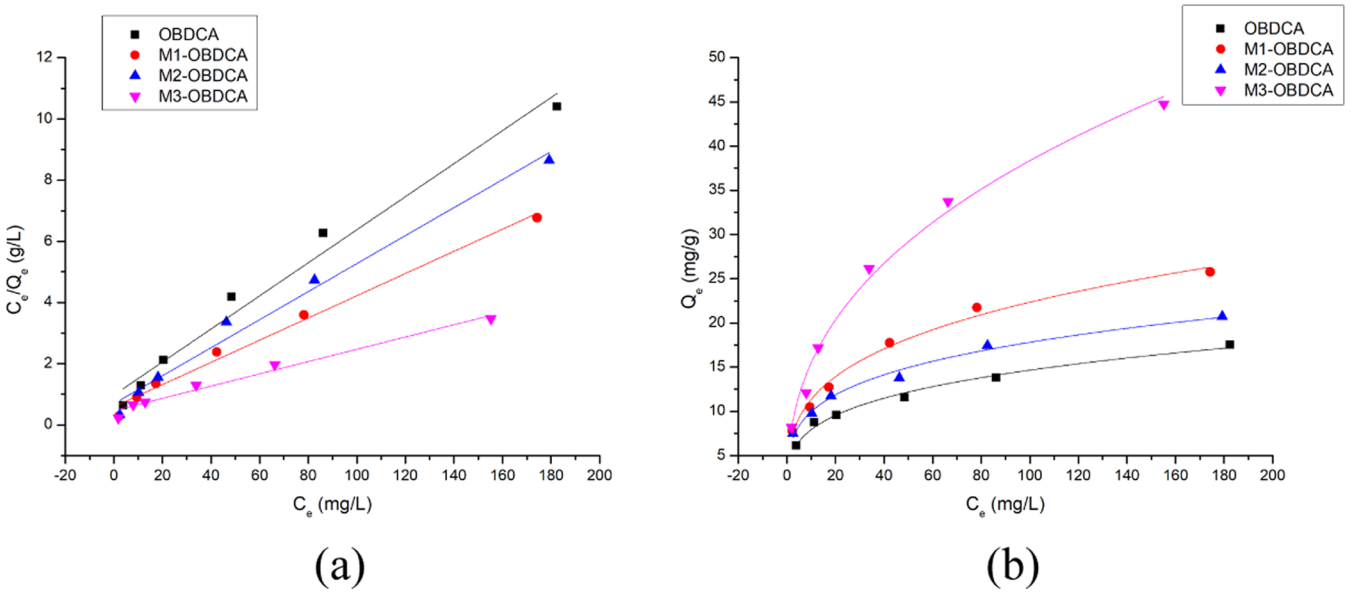

Figure 8. (a) Langmuir and (b) Freundlich model plots. Experimental conditions: dosage of the adsorbent: 1 g/L, pH: 7, reaction time: 180 min, and initial RhB concentration: 10−200 mg/L.

Table 3. Adsorption Isotherm Parameters

	Freundlich		
	k_f	n	R^2
OBDCA	4.3 ± 0.3	0.27 ± 0.01	0.9880
M1-OBDCA	5.8 ± 0.4	0.29 ± 0.02	0.9869
M2-OBDCA	5.6 ± 0.3	0.25 ± 0.01	0.9858
M3-OBDCA	6.3 ± 0.5	0.39 ± 0.03	0.9902
	Langmuir		
	k_l (L/mg)	Q_m (mg/g)	R^2
OBDCA	0.055 ± 0.003	18 ± 1	0.9757
M1-OBDCA	0.061 ± 0.004	30 ± 2	0.9872
M2-OBDCA	0.066 ± 0.002	21 ± 1	0.9822
M3-OBDCA	0.043 ± 0.002	50 ± 3	0.9744

Table 4. Comparison with Other Adsorbents for RhB Adsorption

adsorbent	adsorption capacity (mg/g)	refs
M3-OBDCA	50.32	this study
TMPTA-G-M	45.64	51
ZIF-67/AC	46.2	52
E-spun GO/MIL-101(Fe)/PANCMA NFs	10.46	53
MgO-FCM-NPs	1106	54
NiO/SiO2 nanocomposites	68.0	55

$$Q_t = Q_e(1 - e^{(-k_1 t)}) \quad (3)$$

$$\frac{t}{Q_t} = \frac{1}{k_2 Q_e^{\,2}} + \frac{t}{Q_e} \quad (4)$$

$$Q_t = k_w t^{0.5} + b \quad (5)$$

where Q_e and Q_t are the adsorption capacities (mg/g) at equilibrium and at time t, respectively. k_1 and k_2 are the pseudo-first-order and pseudo-second-order constants, respectively.

The adsorption isotherm of RhB on OBDCA was fitted with the Langmuir and Freundlich models (eqs 6 and 7, respectively).

$$\frac{C_e}{Q_e} = \frac{1}{k_l Q_m} + \frac{C_e}{Q_m} \quad (6)$$

$$Q_e = k_f C_e^{\,n} \quad (7)$$

where Q_m is the theoretic adsorption capacity (mg/g). k_l and k_f are the Langmuir and Freundlich constants, respectively. k_w and b both are intraparticle diffusivity constants.

CONCLUSIONS

OBDCA was modified using HCl, H_2O_2, and H_3PO_4 to enhance the adsorption capacity for organic pollutants. H_2O_2-modified OBDCA showed good adsorption performance for RhB adsorption due to enhanced adsorption sites and the presence of barite and vaterite. The result of adsorption isotherms indicated that the adsorption process belonged to heterogeneous adsorption. The result of adsorption kinetics indicated that the adsorption process was dominated by chemisorption and the adsorption rate was controlled by both the intraparticle diffusion stage and the extraparticle diffusivity stage. Although the adsorption capacity of M3-OBDCA for RhB (50 mg/g) was not at a high level compared with other adsorbents, this study achieved the resource utilization of OBDCA for the treatment of organic pollutants at first.

AUTHOR INFORMATION

Corresponding Authors

Yi Zhang − *State Key Laboratory of Freshwater Ecology and Biotechnology, Institute of Hydrobiology, Chinese Academy of Sciences, Wuhan 430072, China;* orcid.org/0000-0003-4441-3504; Email: zhangyi@ihb.ac.cn

Shibin Xia − *School of Resources and Environmental Engineering, Wuhan University of Technology, Wuhan 430070, China;* orcid.org/0000-0003-4599-7898; Email: xiashibin@126.com

https://doi.org/10.1021/acsomega.1c02214
ACS Omega 2021, 6, 17086−17094

Authors

Yuqing Zhao − *School of Resources and Environmental Engineering, Wuhan University of Technology, Wuhan 430070, China; College of Ecology and Environment, Hubei Vocational College of Ecological Engineering, Wuhan 430200, China; State Key Laboratory of Freshwater Ecology and Biotechnology, Institute of Hydrobiology, Chinese Academy of Sciences, Wuhan 430072, China*

Hang Yang − *School of Resources and Environmental Engineering, Wuhan University of Technology, Wuhan 430070, China*

Jianfa Sun − *China Petroleum & Chemical Corporation, Lichuan 445400, China*

Complete contact information is available at: https://pubs.acs.org/10.1021/acsomega.1c02214

Notes

The authors declare no competing financial interest.

■ ACKNOWLEDGMENTS

The authors sincerely thank the grant funded by the Study on Comprehensive Control of Rocky Desertification and Ecological Service Function Improvement in Karst Peaks (No. 2016YFC0502402) and Fuling Shale Gas Environmental Exploration Technology of National Science and Technology Special Project (Grant No. 2016ZX05060). This work was also financially supported by the National Natural Science Foundation of China (No. 51709254) and Youth Innovation Promotion Association, Chinese Academy of Sciences (No. 2020335)

■ REFERENCES

(1) Frag, E. Y.; Mohamed, N. M.; Elashery, S. E. A. Exploitation of o-benzoyl benzoic acid as an efficient electroactive material for selective determination of Cr (III) ions in pharmaceutical samples and industrial waste water using carbon sensor. *Anal. Chim. Acta* **2021**, *1154*, No. 338322.

(2) Senthil, R. A.; Wu, Y.; Liu, X.; Pan, J. A facile synthesis of nano AgBr attached potato-like Ag2MoO4 composite as highly visible-light active photocatalyst for purification of industrial waste-water. *Environ. Pollut.* **2021**, *269*, No. 116034.

(3) Cong, X.; Zhang, J.; Pu, Y. A novel living environment exposure matrix of the common organic air pollutants for exposure assessment. *Ecotoxicol. Environ. Saf.* **2021**, *215*, No. 112118.

(4) Zhou, K.; Wu, J.; Liu, H. Spatiotemporal variations and determinants of water pollutant discharge in the Yangtze River Economic Belt, China: A spatial econometric analysis. *Environ. Pollut.* **2021**, *271*, No. 116320.

(5) Saravanan, A.; Senthil Kumar, P.; Jeevanantham, S.; Karishma, S.; Tajsabreen, B.; Yaashikaa, P. R.; Reshma, B. Effective water/wastewater treatment methodologies for toxic pollutants removal: Processes and applications towards sustainable development. *Chemosphere* **2021**, *280*, No. 130595.

(6) Thasneema, K. K.; Dipin, T.; Thayyil, M. S.; Sahu, P. K.; Messali, M.; Rosalin, T.; Elyas, K. K.; Saharuba, P. M.; Anjitha, T.; Hadda, T. B. Removal of toxic heavy metals, phenolic compounds and textile dyes from industrial waste water using phosphonium based ionic liquids. *J. Mol. Liq.* **2021**, *323*, No. 114645.

(7) Razak, M. R.; Yusof, N. A.; Aris, A. Z.; Nasir, H. M.; Haron, M. J.; Ibrahim, N. A.; Johari, I. S.; Kamaruzaman, S. Phosphoric acid modified kenaf fiber (K-PA) as green adsorbent for the removal of copper (II) ions towards industrial waste water effluents. *React. Funct. Polym.* **2020**, *147*, No. 104466.

(8) Raza, W.; Lee, J.; Raza, N.; Luo, Y.; Kim, K.-H.; Yang, J. Removal of phenolic compounds from industrial waste water based on membrane-based technologies. *J. Ind. Eng. Chem.* **2019**, *71*, 1−18.

(9) Geng, J.; Chang, J. Synthesis of magnetic Forsythia suspensa leaf powders for removal of metal ions and dyes from wastewater. *J. Environ. Chem. Eng.* **2020**, *8*, No. 104224.

(10) Sun, Z.; Yang, J.; Qi, Y.; Wang, F.; Hong, W.; Li, H.; Jiang, Y. Facile preparation of hydroxyl-rich mesoporous magnesium silicate with excellent adsorption performance. *Surf. Interfaces* **2020**, *20*, No. 100519.

(11) Liang, Y.; Huang, G.; Zhang, Q.; Yang, Y.; Zhou, J.; Cai, J. Hierarchical porous carbons from biowaste: Hydrothermal carbonization and high-performance for Rhodamine B adsorptive removal. *J. Mol. Liq.* **2021**, *330*, No. 115580.

(12) Vigneshwaran, S.; Sirajudheen, P.; Karthikeyan, P.; Meenakshi, S. Fabrication of sulfur-doped biochar derived from tapioca peel waste with superior adsorption performance for the removal of Malachite green and Rhodamine B dyes. *Surf. Interfaces* **2021**, *23*, No. 100920.

(13) Vigneshwaran, S.; Park, C. M.; Meenakshi, S. Designed fabrication of sulfide-rich bi-metallic-assembled MXene layered sheets with dramatically enhanced photocatalytic performance for Rhodamine B removal. *Sep. Purif. Technol.* **2021**, *258*, No. 118003.

(14) Song, C.; Wang, L.-j.; Sun, S.-m.; Wu, Y.; Xu, L.-j.; Gan, L. Preparation of visible-light photocatalysts of Bi2O3/Bi embedded in porous carbon from Bi-based metal organic frameworks for highly efficient Rhodamine B removal from water. *Carbon* **2021**, *174*, 760.

(15) Gan, L.; Geng, A.; Song, C.; Xu, L.; Wang, L.; Fang, X.; Han, S.; Cui, J.; Mei, C. Simultaneous removal of rhodamine B and Cr(VI) from water using cellulose carbon nanofiber incorporated with bismuth oxybromide: The effect of cellulose pyrolysis temperature on photocatalytic performance. *Environ. Res.* **2020**, *185*, No. 109414.

(16) Abdel-Aziz, R.; Ahmed, M. A.; Abdel-Messih, M. F. A novel UV and visible light driven photocatalyst AgIO4/ZnO nanoparticles with highly enhanced photocatalytic performance for removal of rhodamine B and indigo carmine dyes. *J. Photochem. Photobiol., A* **2020**, *389*, No. 112245.

(17) Yang, S.; Feng, Y.; Liu, N.; Zhao, Y.; Wang, X.; Zhang, Z.; Chen, H.; Yu, Y. Enhancement on the removal of Rhodamine B (RhB) by means of the Enlarged Anode Electric Biological (EAEB) reactor. *Chemosphere* **2020**, *245*, No. 125566.

(18) He, Y.; Lv, H.; Daili, Y.; Yang, Q.; Junior, L. B.; Liu, D.; Liu, H.; Ma, Z. Construction of a new cascade photogenerated charge transfer system for the efficient removal of bio-toxic levofloxacin and rhodamine B from aqueous solution: Mechanism, degradation pathways and intermediates study. *Environ. Res.* **2020**, *187*, No. 109647.

(19) Shi, P.; Hu, X.; Wang, Y.; Duan, M.; Fang, S.; Chen, W. A PEG-tannic acid decorated microfiltration membrane for the fast removal of Rhodamine B from water. *Sep. Purif. Technol.* **2018**, *207*, 443−450.

(20) Hou, Y.; Huang, G.; Li, J.; Yang, Q.; Huang, S.; Cai, J. Hydrothermal conversion of bamboo shoot shell to biochar: Preliminary studies of adsorption equilibrium and kinetics for rhodamine B removal. *J. Anal. Appl. Pyrolysis* **2019**, *143*, No. 104694.

(21) Bethi, B.; Manasa, V.; Srinija, K.; Sonawane, S. H. Intensification of Rhodamine-B dye removal using hydrodynamic cavitation coupled with hydrogel adsorption. *Chem. Eng. Process.* **2018**, *134*, 51−57.

(22) Rachna, K.; Agarwal, A.; Singh, N. B. Preparation and characterization of zinc ferrite—Polyaniline nanocomposite for removal of rhodamine B dye from aqueous solution. *Environ. Nanotechnol. Monit. Manage.* **2018**, *9*, 154−163.

(23) Chen, X.; Li, H.; Liu, W.; Zhang, X.; Wu, Z.; Bi, S.; Zhang, W.; Zhan, H. Effective removal of methyl orange and rhodamine B from aqueous solution using furfural industrial processing waste: Furfural residue as an eco-friendly biosorbent. *Colloids Surf., A* **2019**, *583*, No. 123976.

(24) Zhao, Y.; Zhu, L.; Li, W.; Liu, J.; Liu, X.; Huang, K. Insights into enhanced adsorptive removal of Rhodamine B by different

chemically modified garlic peels: Comparison, kinetics, isotherms, thermodynamics and mechanism. *J. Mol. Liq.* **2019**, *293*, No. 111516.
(25) Wang, C.-q.; Lin, X.-y.; He, M.; Wang, D.; Zhang, S.-l. Environmental performance, mechanical and microstructure analysis of concrete containing oil-based drilling cuttings pyrolysis residues of shale gas. *J. Hazard. Mater.* **2017**, *338*, 410−427.
(26) Ikotun, J. O.; Okeniyi, J. O.; Akinlabi, E. T.; Akinlabi, S. A.; Okeniyi, E. T.; Olanrewaju, D. O. Physicochemical and mineralogical characterization datasets from oil drill cuttings in comparison with other cement types for cement partial-replacement in concrete. *Chem. Data Collect.* **2019**, *19*, No. 100176.
(27) Wang, C.-q.; Lin, X.-y.; Mei, X.-d.; Luo, X.-g. Performance of non-fired bricks containing oil-based drilling cuttings pyrolysis residues of shale gas. *J. Cleaner Prod.* **2019**, *206*, 282−296.
(28) Yang, H.; Huang, S.; Zhang, Y.; Zhou, B.; Manzoor Ahmed, S.; Liu, H.; Liu, Y.; He, Y.; Xia, S. Remediation effect of Cr (VI)-contaminated soil by secondary pyrolysis oil-based drilling cuttings ash. *Chem. Eng. J.* **2020**, *398*, No. 125473.
(29) Liuyang, X.; Yang, H.; Huang, S.; Zhang, Y.; Xia, S. Resource utilization of secondary pyrolysis oil-based drilling cuttings ash for removing Cr (VI) contaminants: Adsorption properties, kinetics and mechanism. *J. Environ. Chem. Eng.* **2020**, *8*, No. 104474.
(30) Mobarak, M.; Selim, A. Q.; Mohamed, E. A.; Seliem, M. K. Modification of organic matter-rich clay by a solution of cationic surfactant/H2O2: A new product for fluoride adsorption from solutions. *J. Cleaner Prod.* **2018**, *192*, 712−721.
(31) Chen, M.; Wang, F.; Zhang, D.-l.; Yi, W.-m.; Liu, Y. Effects of acid modification on the structure and adsorption NH4+-N properties of biochar. *Renewable Energy* **2021**, *169*, 1343−1350.
(32) Wei, F.; Guo, X.; Liao, J.; Bao, W.; Chang, L. Ultra-deep removal of thiophene in coke oven gas over Y zeolite: Effect of acid modification on adsorption desulfurization. *Fuel Process. Technol.* **2021**, *213*, No. 106632.
(33) Ahmad, M. A.; Eusoff, M. A.; Oladoye, P. O.; Adegoke, K. A.; Bello, O. S. Statistical optimization of Remazol Brilliant Blue R dye adsorption onto activated carbon prepared from pomegranate fruit peel. *Chem. Data Collect.* **2020**, *28*, No. 100426.
(34) Ghosh, I.; Kar, S.; Chatterjee, T.; Bar, N.; Das, S. K. Adsorptive removal of Safranin-O dye from aqueous medium using coconut coir and its acid-treated forms: Adsorption study, scale-up design, MPR and GA-ANN modeling. *Sustainable Chem. Pharm.* **2021**, *19*, No. 100374.
(35) Chanajaree, R.; Sriuttha, M.; Lee, V. S.; Wittayanarakul, K. Thermodynamics and kinetics of cationic/anionic dyes adsorption on cross-linked chitosan. *J. Mol. Liq.* **2020**, *322*, No. 114507.
(36) Xia, J.; Gao, Y.; Yu, G. Tetracycline removal from aqueous solution using zirconium-based metal-organic frameworks (Zr-MOFs) with different pore size and topology: Adsorption isotherm, kinetic and mechanism studies. *J. Colloid Interface Sci.* **2021**, *590*, 495−505.
(37) Siyal, A. A.; Shamsuddin, M. R.; Rabat, N. E.; Zulfiqar, M.; Man, Z.; Low, A. Fly ash based geopolymer for the adsorption of anionic surfactant from aqueous solution. *J. Cleaner Prod.* **2019**, *229*, 232−243.
(38) Wang, Z.; Wu, H.; Xu, Y.; Shu, K.; Yang, J.; Luo, L.; Xu, L. Effect of dissolved fluorite and barite species on the flotation and adsorption behavior of bastnaesite. *Sep. Purif. Technol.* **2020**, *237*, No. 116387.
(39) Song, X.; Cao, Y.; Bu, X.; Luo, X. Porous vaterite and cubic calcite aggregated calcium carbonate obtained from steamed ammonia liquid waste for Cu2+ heavy metal ions removal by adsorption process. *Appl. Surf. Sci.* **2021**, *536*, No. 147958.
(40) Nagpal, M.; Kakkar, R. Selective adsorption and separation of toxic cationic dyes using hierarchically porous SDBS modified vaterite microspheres (Hr-SMV). *J. Phys. Chem. Solids* **2020**, *146*, No. 109598.
(41) Chen, Y.-Y.; Yu, S.-H.; Jiang, H.-F.; Yao, Q.-Z.; Fu, S.-Q.; Zhou, G.-T. Performance and mechanism of simultaneous removal of Cd(II) and Congo red from aqueous solution by hierarchical vaterite spherulites. *Appl. Surf. Sci.* **2018**, *444*, 224−234.
(42) Khalilzadeh Shirazi, E.; Metzger, J. W.; Fischer, K.; Hassani, A. H. Removal of textile dyes from single and binary component systems by Persian bentonite and a mixed adsorbent of bentonite/charred dolomite. *Colloids Surf., A* **2020**, *598*, No. 124807.
(43) Sun, Z.; Huang, D.; Duan, X.; Hong, W.; Liang, J. Functionalized nanoflower-like hydroxyl magnesium silicate for effective adsorption of aflatoxin B1. *J. Hazard. Mater.* **2020**, *387*, No. 121792.
(44) Wang, X.; Chen, S.; Sun, J.; Zhang, D.; Yan, Z.; Xu, X.; Song, J. Synthesis of large pore sized mesoporous carbon using alumina-templated strategy for high-performance RhB removal. *Microporous Mesoporous Mater.* **2021**, *318*, No. 110993.
(45) Mishra, S.; Sahoo, S. S.; Debnath, A. K.; Muthe, K. P.; Das, N.; Parhi, P. Cobalt ferrite nanoparticles prepared by microwave hydrothermal synthesis and adsorption efficiency for organic dyes: Isotherms, thermodynamics and kinetic studies. *Adv. Powder Technol.* **2020**, *31*, 4552−4562.
(46) Zhao, S.; Zhan, Y.; Wan, X.; He, S.; Yang, X.; Hu, J.; Zhang, G. Selective and efficient adsorption of anionic dyes by core/shell magnetic MWCNTs nano-hybrid constructed through facial polydopamine tailored graft polymerization: Insight of adsorption mechanism, kinetic, isotherm and thermodynamic study. *J. Mol. Liq.* **2020**, *319*, No. 114289.
(47) Chen, J.; Liao, Y.; Wan, X.; Tie, S.; Zhang, B.; Lan, S.; Gao, X. A high performance MoO3@MoS2 porous nanorods for adsorption and photodegradation of dye. *J. Solid State Chem.* **2020**, *291*, No. 121652.
(48) Naushad, M.; Alqadami, A. A.; Al-Kahtani, A. A.; Ahamad, T.; Awual, M. R.; Tatarchuk, T. Adsorption of textile dye using para-aminobenzoic acid modified activated carbon: Kinetic and equilibrium studies. *J. Mol. Liq.* **2019**, *296*, No. 112075.
(49) Değermenci, G. D.; Değermenci, N.; Ayvaoğlu, V.; Durmaz, E.; Çakır, D.; Akan, E. Adsorption of reactive dyes on lignocellulosic waste; characterization, equilibrium, kinetic and thermodynamic studies. *J. Cleaner Prod.* **2019**, *225*, 1220−1229.
(50) Utilization of Cr-Contaminated Oil-Based Drilling-Cuttings Ash in Preparation of Bauxite-Based Proppants. *Environ. Eng. Sci.*.
(51) Yang, Z.; Wu, G.; Gan, C.; Cai, G.; Zhang, J.; Ji, H. Effective adsorption of arsenate, dyes and eugenol from aqueous solutions by cationic supramolecular gel materials. *Colloids Surf., A* **2021**, *616*, No. 126238.
(52) Li, Y.; Yan, X.; Hu, X.; Feng, R.; Zhou, M. Trace pyrolyzed ZIF-67 loaded activated carbon pellets for enhanced adsorption and catalytic degradation of Rhodamine B in water. *Chem. Eng. J.* **2019**, *375*, No. 122003.
(53) Huang, Z.; Lai, Z.; Zhu, D.; Wang, H.; Zhao, C.; Ruan, G.; Du, F. Electrospun graphene oxide/MIL-101(Fe)/poly(acrylonitrile-co-maleic acid) nanofiber: A high-efficient and reusable integrated photocatalytic adsorbents for removal of dye pollutant from water samples. *J. Colloid Interface Sci.* **2021**, *597*, 196−205.
(54) Rahdar, S.; Rahdar, A.; Zafar, M. N.; Shafqat, S. S.; Ahmadi, S. Synthesis and characterization of MgO supported Fe−Co−Mn nanoparticles with exceptionally high adsorption capacity for Rhodamine B dye. *J. Mater. Res. Technol.* **2019**, *8*, 3800−3810.
(55) Rubab, R.; Ali, S.; Rehman, A. U.; Khan, S. A.; Khan, A. M. Templated synthesis of NiO/SiO2 nanocomposite for dye removal applications: Adsorption kinetics and thermodynamic properties. *Colloids Surf., A* **2021**, *615*, No. 126253.

https://doi.org/10.1021/acsomega.1c02214
ACS Omega 2021, 6, 17086−17094